Research in
Astronomy and
Astrophysics

Size distribution of galaxies in SDSS DR7: weak dependence on halo environment

You-Cai Zhang[1] and Xiao-Hu Yang[2,3]

[1] Key Laboratory for Research in Galaxies and Cosmology, Shanghai Astronomical Observatory, Shanghai 200030, China; *yczhang@shao.ac.cn*
[2] Department of Astronomy, Shanghai Key Laboratory for Particle Physics and Cosmology, Shanghai Jiao Tong University, Shanghai 200240, China
[3] IFSA Collaborative Innovation Center, and Tsung-Dao Lee Institute, Shanghai Jiao Tong University, Shanghai 200240, China

Abstract Using a sample of galaxies selected from the Sloan Digital Sky Survey Data Release 7 (SDSS DR7) and a catalog of bulge-disk decompositions, we study how the size distribution of galaxies depends on the intrinsic properties of galaxies, such as concentration, morphology, specific star formation rate (sSFR), and bulge fraction, and on the large-scale environments in the context of central/satellite decomposition, halo environment, the cosmic web: `cluster`, `filament`, `sheet` and `void`, as well as galaxy number density. We find that there is a strong dependence of the luminosity- or mass-size relation on the galaxy concentration, morphology, sSFR and bulge fraction. Compared with late-type (spiral) galaxies, there is a clear trend of smaller sizes and steeper slope for early-type (elliptical) galaxies. Similarly, galaxies with a high bulge fraction have smaller sizes and steeper slopes than those with a low bulge fraction. Fitting formulae of the average luminosity- and mass-size relations are provided for galaxies with these different intrinsic properties. Examining galaxies in terms of their large scale environments, we find that the mass-size relation has some weak dependence on the halo mass and central/satellite segregation for galaxies within mass range $9.0 \leq \log M_* \leq 10.5$, where satellites or galaxies in more massive halos have slightly smaller sizes than their counterparts, while the cosmic web and local number density dependence of the mass-size relation is almost negligible.

Key words: large-scale structure of universe — methods: statistical — cosmology: observations

1 INTRODUCTION

In the current paradigm of galaxy formation, galaxies are considered to form from the accretion of gas in the gravitational potential well provided by dark matter (White & Rees 1978). According to the tidal torque theory, dark matter and gas acquire their angular momenta by the interaction between the inertia tensor and the local tidal field (Peebles 1969; White 1984). In this scheme, the rotational disks are assumed to form from the collapse of gas in dark matter halos (Fall & Efstathiou 1980; Fall 1983). In the model for the formation of a galactic disk formulated by Mo et al. (1998), the present-day disks assembled recently at $z \leq 1$. Disks at high redshift are small and dense, and could merge together to form elliptical galaxies.

As one of the fundamental observational properties, the sizes of galaxies are useful for calibrating the galaxy evolution models (de Jong & Lacey 2000; Khochfar & Silk 2006; Trujillo et al. 2006, 2007; Buitrago et al. 2008; Hopkins et al. 2010; Romanowsky & Fall 2012; Cappellari et al. 2013; Fall & Romanowsky 2013; Javanmardi & Kroupa 2017; Hill et al. 2017; Yıldırım et al. 2017). The sizes of galaxies are well known to be correlated with their stellar mass (or luminosity). Over the past few decades, a number of authors have studied the luminosity- or mass-size relation of galaxies (Shen et al. 2003; Trujillo et al.

2004; Guo et al. 2009; Lange et al. 2015; Chan et al. 2016; Sweet et al. 2017; Furlong et al. 2017). It is found that the relationship between size and mass is strongly dependent on the morphology of the galaxy. At fixed stellar mass, early-type (elliptical) galaxies have smaller sizes than late-type (spiral) galaxies. In previous studies, the mass-size relation has been fitted using a single or double power law formula. For early-type galaxies, Shen et al. (2003) used a single power law formula to fit the mass-size relation (see also van der Wel et al. 2008; Bottrell et al. 2017). However, some studies showed that the most massive part of the mass-size relation is curved in such a way that the mass-size relation of the most massive galaxies has a larger slope than that of low-mass galaxies (Desroches et al. 2007; Hyde & Bernardi 2009; Bernardi et al. 2011; Furlong et al. 2017). The steeper slope at the high-mass end is likely caused by the larger sizes of central galaxies in clusters, i.e. cD galaxies, which have a very extended luminosity profile so that they have larger sizes than normal ellipticals at the same stellar mass. In this case, the mass-size relation of early-type (elliptical) galaxies can be fitted well by a double power law formula. For late-type galaxies, most of the studies used the double power law formula to fit the mass-size relation (e.g., Shen et al. 2003; Dutton et al. 2011), whereas some authors used a single power law formula (e.g., Dutton et al. 2007; Bottrell et al. 2017). In view of this, both single and double power law functions are used by Lange et al. (2015, 2016). They claimed that the single power law formula is sufficient to describe the mass-size relation of late-type galaxies, whereas the double power law is more robust than single power law to fit early-type galaxies (see table 2 of Lange et al. 2016).

More recently, a growing number of authors have endeavored to examine the environmental dependence of the mass-size relation. Generally, the environmental dependence of the luminosity- or mass-size relation is controversial. On one hand, several studies have claimed that there is no environmental dependence of the mass-size relation (Rettura et al. 2010; Maltby et al. 2010; Nair et al. 2010; Huertas-Company et al. 2013; Kelkar et al. 2015; Saracco et al. 2017). Using 45 massive ($M_* > 5 \times 10^{10}\,M_\odot$) early-type galaxies at $z \sim 1.2$, Rettura et al. (2010) found that early-type galaxies, both in clusters and in the field, follow a similar mass-size relation. Using a sample of ~ 1200 field and cluster galaxies, Maltby et al. (2010) showed that there is no environmental dependence for elliptical galaxies and for high-mass spiral galaxies ($M_* > 10^{10}\,M_\odot$). Using 12 150 Sloan Digital Sky Survey (SDSS) galaxies with visual classification, Nair et al. (2010) showed that

the slope of the luminosity-size relation seems independent of environmental density. Using a sample of $\sim 12\,000$ local early-type galaxies from SDSS Data Release 7 (DR7), Huertas-Company et al. (2013) claimed that galaxies in clusters have similar sizes as the ones in the field. Using ~ 1500 galaxies at $0.4 < z < 0.8$ from the ESO Distant Cluster Survey, Kelkar et al. (2015) found that there is no significant difference in the size distributions of cluster and field galaxies. Comparing a sample of 56 elliptical galaxies in clusters at $z \sim 1.3$ with ~ 430 field galaxies from GOODS, COSMOS and CANDELS, Saracco et al. (2017) found that there is no difference in the size at a fixed mass of galaxies in clusters and in the field.

On the other hand, there are a number of studies suggesting that the sizes of galaxies are dependent on their environments. Some studies claimed that early-type galaxies in clusters are larger than their counterparts in the field (Papovich et al. 2012; Bassett et al. 2013; Lani et al. 2013; Strazzullo et al. 2013; Delaye et al. 2014; Yoon et al. 2017). Using < 100 galaxies at $z \sim 1.6$ from CANDELS observations, Papovich et al. (2012) and Bassett et al. (2013) claimed that quiescent galaxies in clusters are on average larger compared with those in the field. Using $\sim 96\,000$ galaxies from the UKIDSS Ultra Deep Survey, Lani et al. (2013) showed that passive galaxies in a high density environment are on average significantly larger at $1 < z < 2$. Using ~ 12 galaxies in an X-ray-detected galaxy cluster at $z \sim 2$, Strazzullo et al. (2013) found that passive early-type galaxies are larger by a factor of ~ 2 in clusters than in the field. Using a sample of ~ 400 quiescent early-type galaxies at $0.8 < z < 1.5$, Delaye et al. (2014) claimed that the average sizes of galaxies in clusters are 30%–40% larger than the ones in the field. In a recent study, Yoon et al. (2017) found that early-type galaxies with mass larger than $10^{11.2}\,M_\odot$ in high-density environments are as much as 20%–40% larger than those in low-density environments, using 73 116 early-type galaxies at $0.1 \leq z < 0.15$ from SDSS DR7. However, some studies indicated that galaxies in the field are larger than the ones in clusters (Raichoor et al. 2012; Poggianti et al. 2013; Cebrián & Trujillo 2014; Pranger et al. 2017). Using a sample of 76 early-type galaxies at $z \sim 1.3$, Raichoor et al. (2012) found that galaxies in clusters are smaller than field galaxies. Using a complete sample of galaxies at $0.03 \leq z \leq 0.11$, Poggianti et al. (2013) indicated that galaxies in the field are larger than in clusters. Based on galaxies from SDSS DR7, Cebrián & Trujillo (2014) found that galaxies are larger in less-dense regions than in high-density regions. Using about 700 low-redshift ($z < 0.063$) disk galaxies

from SDSS DR7, Pranger et al. (2017) found that the sizes of galaxies are smaller by $\sim 15\%$ in clusters than in the field.

In this study, using a sample of galaxies selected from SDSS DR7 (Blanton et al. 2005) and a catalog of bulge-disk decompositions (Simard et al. 2011), we investigate how the luminosity- or mass-size relation depends on the intrinsic properties of galaxies, such as concentration, morphology, specific star formation rate (sSFR) and bulge fraction, and on the large-scale environments in the context of central/satellite decomposition, halo environment, the cosmic web: `cluster`, `filament`, `sheet` and `void`, as well as galaxy number density. Here the cosmic web environments are determined according to the eigenvalues of the tidal field, constructed from the largest continuous region from SDSS DR7 (Hahn et al. 2007a,b; Wang et al. 2012), while the central/satellite separation and halo mass environment are calculated using galaxy groups constructed by Yang et al. (2007).

This paper is organized as follows. In Section 2, we describe the observational data, including galaxies from the NYU Value-Added Galaxy Catalog (NYU-VAGC) and galaxies from bulge-disk decomposition samples. In Section 3, we present how the luminosity- or mass-size relation depends on galaxy morphology, bulge fraction and large-scale environments. Finally, we summarize and discuss our results in Section 5. Unless stated otherwise, we adopt a ΛCDM cosmology with parameters from Planck Collaboration et al. (2016): $\Omega_{\mathrm{m}} = 0.308$, $\Omega_{\Lambda} = 0.692$, $n_{\mathrm{s}} = 0.968$, $h = H_0/(100\,\mathrm{km\,s^{-1}\,Mpc^{-1}}) = 0.678$ and $\sigma_8 = 0.815$.

2 OBSERVATIONAL DATA

In this section we describe the observational data we have used to investigate the luminosity- or mass-size relations of galaxies. Galaxies used in this paper come from the SDSS (York et al. 2000), which has become one of the most successful surveys in the history of astronomy. SDSS has provided the most detailed three-dimensional maps of the Universe, with deep multi-band images and spectra for more than three million astronomical objects.

2.1 NYU Value-Added Galaxy Catalog

The galaxy sample used here is from the New York University Value-Added Galaxy Catalog[1] (NYU-VAGC; Blanton et al. 2005), which is based on the multi-band imaging and spectroscopic survey SDSS DR7 (Abazajian

---

[1] *http://sdss.physics.nyu.edu/vagc/*

et al. 2009). From the NYU-VAGC, we collect a total of 639 359 galaxies with redshifts in the range $0.01 \leq z \leq 0.2$ and with redshift completeness $\mathcal{C}_z > 0.7$. For each galaxy, the r-band absolute magnitude M_r was computed, which was K-corrected and evolution corrected to $z = 0.1$ using the method described by Blanton et al. (2003) and Blanton & Roweis (2007). In addition to the r-band absolute magnitudes, we also use the stellar masses of galaxies. Here the stellar masses and star formation rates (SFRs) of galaxies are obtained from the public catalog provided by Chang et al. (2015), in which we only use a total of 633 205 galaxies that have reliable aperture corrections (FLAG = 1).

In the NYU-VAGC catalog, the Petrosian half-light radii R_{50} and R_{90} are the radii enclosing 50% and 90% of the Petrosian flux, respectively. The Petrosian flux F_{P} in any band is defined as the flux within a certain number N_{P} ($N_{\mathrm{P}} = 2.0$ in SDSS) of the Petrosian radius r_{P},

$$F_{\mathrm{P}} = \int_0^{N_{\mathrm{P}} r_{\mathrm{P}}} 2\pi r I(r)\mathrm{d}r \ , \qquad (1)$$

where $I(r)$ is the azimuthally averaged surface brightness profile, and r_{P} is defined as the radius at which the Petrosian ratio R_{P} equals some specified value ($R_{\mathrm{P}} = 0.2$ in SDSS). The Petrosian ratio R_{P} is defined as the ratio of the local surface brightness in an annulus to the mean surface brightness within the radius r_{P}, which can be expressed by (Blanton et al. 2001; Yasuda et al. 2001),

$$R_{\mathrm{P}} = \frac{\int_{0.8r_{\mathrm{P}}}^{1.25r_{\mathrm{P}}} 2\pi r I(r)\mathrm{d}r/[\pi(1.25^2 - 0.8^2)r_{\mathrm{P}}^2]}{\int_0^{r_{\mathrm{P}}} 2\pi r I(r)\mathrm{d}r/(\pi r_{\mathrm{P}}^2)} \ . \qquad (2)$$

Given the radii R_{50} and R_{90}, the concentration index of the galaxy is defined as $c = R_{90}/R_{50}$, which is correlated with galaxy morphological type. As shown in Shen et al. (2003), SDSS galaxies may suffer a small fraction of incompleteness in sizes of galaxies, due to very compact galaxies or very low surface brightness galaxies. In order to consider the effect of incompleteness on the luminosity-size relation, we have drawn two reference lines (black dashed lines) in the left panel of Figure 1, one is the $\mu_{\mathrm{max}} = 23.0\,\mathrm{mag\,arcsec^{-2}}$, which corresponds to the very low surface brightness galaxies, and the other is $\mu_{\mathrm{min}} = 18.5\,\mathrm{mag\,arcsec^{-2}}$, which may correspond to a galaxy with $R_{50} = 2.0''$ and apparent magnitude $m_r = 15$. As shown in the left panel of Figure 1, most of the galaxies in our samples are inside the two reference lines, which means that the incompleteness has almost no effect on the luminosity- or mass-size relations, however, the faint late-type galaxies ($c < 2.85$) with $M_r > -18.0$ could be slightly biased by the incompleteness. Besides,

we also adopt the morphological classifications of galaxies from the Galaxy Zoo 2 Catalog (GZ2; Willett et al. 2013), which provides the most common classification for a galaxy with $gz2\_class$ strings. Elliptical and spiral galaxies have $gz2\_class$ strings beginning with 'E' and 'S', respectively. This results in 107 230 elliptical galaxies and 134 024 spiral galaxies cross-identified in our NYU-VAGC sample.

We also make use of the galaxy sample with bulge-disk decompositions in the r-band for 1.12 million galaxies from SDSS DR7 (Simard et al. 2011). In their model, the galaxy image is fitted by the sum of a pure exponential disk and a de Vaucouleurs bulge (Sérsic index n_b). For comparison, Simard et al. (2011) applied three different fitting models: an $n_b = 4$ bulge-disk model, a free-n_b bulge-disk model and a pure Sérsic model. In the following analysis, we adopt the galaxy structure parameters from their canonical $n_b = 4$ bulge-disk fitting model using the GIM2D software package. In this paper, the galaxy parameters we employed are the r-band galaxy circular half-light radius $R_{\rm chl}$ and the bulge-to-total ratio B/T (see table 1 in Simard et al. (2011)). From Simard et al. (2011)'s database, 586 938 (about 91.8%) galaxies can be cross identified within a total of 639 359 galaxies in our SDSS DR7 galaxy catalog.

2.2 The Large Scale Environments

Based on the adaptive halo-based group finder developed by Yang et al. (2005, 2007), we construct a sample of 472 416 groups, among which 404 246 groups are single galaxies. Using the complete galaxy groups with masses $M_{\rm h} \geq 10^{12} h^{-1} M_\odot$, Wang et al. (2012) constructed the tidal field $T_{i,j}$ with a smoothing scale $R_s = 2.1 \, h^{-1} \, {\rm Mpc}$. According to the number of positive eigenvalues associated with the local tidal tensor, the group's environment is classified into one of four cosmic web types: cluster, filament, sheet and void (Hahn et al. 2007a,b; Forero-Romero et al. 2009; Zhang et al. 2009, 2013, 2015). If all of the three eigenvalues at the position of the group are positive, the group is classified into cluster, while the case of two, one or zero positive numbers of eigenvalues corresponds to filament, sheet or void, respectively. In order to ensure sample completeness, the galaxy's environment classification is limited in the largest continuous region in the Northern Galactic Cap of SDSS DR7, which results in 117 667 galaxies located in cluster, 212 075 galaxies in filament, 61 666 galaxies in sheet and 4496 in void.

Figure 2 shows the spatial distribution of galaxies in a $200 \, h^{-1} \, {\rm Mpc} \times 200 \, h^{-1} \, {\rm Mpc}$ slice of thickness $20 \, h^{-1} \, {\rm Mpc}$, in which galaxies in different environments are indicated by different colors: cluster (red), filament (orange), sheet (green) and void (blue).

In addition to the halo environment and cosmic web environment, we also calculate the local (surface) number density of galaxies. The surface number density of each galaxy is calculated by counting nearby galaxies in a volume-limited sample within the redshift range $0.01 < z < 0.12$ and with the magnitude $M_r < -21.0$. For each galaxy in the redshift range $0.01 < z < 0.12$, we calculate the surface number density by

$$\Sigma = n/\pi r^2 \, , \qquad (3)$$

where n is the galaxy counts ($M_r < -21.0$) in a cylinder of radius r and line-of-sight length Δv. The unit of the surface number density is $h^{-1} \, {\rm Mpc}^{-2}$.

3 DEPENDENCE ON GALAXY PROPERTIES

In this section, we investigate how the luminosity- or mass-size relation depends on the intrinsic properties of galaxies, such as concentration, morphology, sSFR, bulge fraction and surface brightness.

3.1 Dependence on Concentration

The concentration index, $c = R_{90}/R_{50}$, is found to be tightly correlated with galaxy morphological type (Shimasaku et al. 2001; Shen et al. 2003; Park & Choi 2005; Deng 2013; Deng & Yu 2015). Shimasaku et al. (2001) demonstrated that the concentration index can be used to classify galaxies into early and late types with their recommended choice of $c = 3.03$. Nakamura et al. (2003) separated galaxies into early and late types with $c = 2.857$. They claimed that this choice of the concentration index $c = 2.857$ can minimize contamination of the opposite morphological type. Shen et al. (2003) used $c = 2.86$ to separate galaxies into early and late types. Based on SDSS DR8, Deng (2013) claimed that the concentration index $c = 2.85$ can be used to construct a reasonably pure late-type galaxy sample, although it is unfortunately not good enough to construct an early-type galaxy sample. In this paper, we separate galaxies into early and late types according to $c \geq 2.85$ and $c < 2.85$. In the r-band absolute magnitude range $-24.0 \leq M_r \leq -15.5$, the early-type subsample ($c \geq 2.85$) contains 214 950 galaxies, while the late-type subsample ($c < 2.85$) contains 424 363 galaxies.
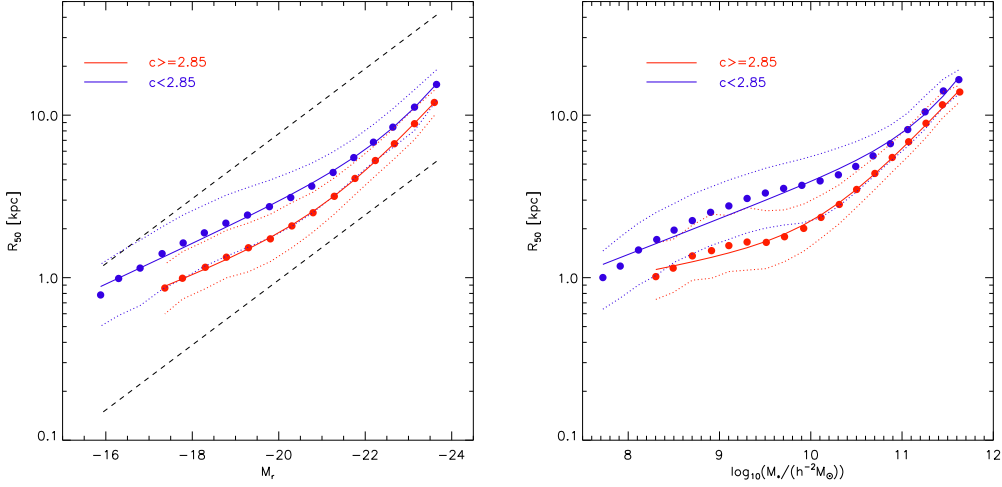
Fig. 1 Galaxy Petrosian half-light radius R_{50} as a function of r-band absolute magnitude and stellar mass of galaxies in the NYU-VAGC samples. The *red* and *blue solid points* are median values of R_{50} for galaxies with different concentration ($c \geq 2.85$ and $c < 2.85$), and the corresponding *dotted lines* correspond to 16 and 84 percentiles. The *solid lines* show the fitting results using Equations (4) and (5), respectively. The *black dashed lines* correspond to the reference lines with $\mu_{\max} = 23.0\,\mathrm{mag\,arcsec}^{-2}$ and $\mu_{\min} = 18.5\,\mathrm{mag\,arcsec}^{-2}$.
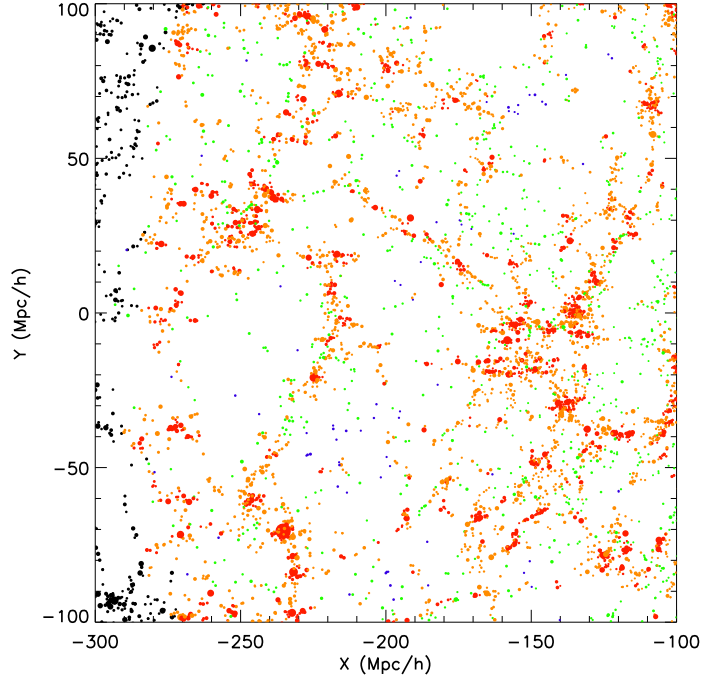
Fig. 2 Spatial distribution of galaxies in different environments in a slice of thickness $20\,h^{-1}\,\mathrm{Mpc}$ from SDSS DR7. The symbol sizes of the galaxies are proportional to their luminosities. The galaxies in four different environments are indicated by different colors: `cluster` (*red*), `filament` (*orange*), `sheet` (*green*) and `void` (*blue*). *Black dots* are galaxies outside the limited continuous volume, and are therefore not included in the analysis.

Based on these galaxy samples, we investigate the dependence of the luminosity-size relation on the galaxy concentration index.

In the left panel of Figure 1, we show the galaxy Petrosian half-light radius R_{50} as a function of r-band absolute magnitude M_r of galaxies in the NYU-VAGC sam-

ples from SDSS DR7. The size distribution of galaxies at a given luminosity (or stellar mass) can be well described by a log-normal distribution with the median value of R_{50}. Therefore, in this paper we use the median values of R_{50} to characterize the sizes of galaxies in each magnitude (or mass) bin. In Figure 1, the red and blue solid dots signify

the median values of R_{50} for early-type ($c \geq 2.85$) and late-type ($c < 2.85$) galaxies, respectively, with the corresponding dotted lines representing 16 and 84 percentiles.

As shown in Figure 1, the luminosity-size relations are quite different for early-type and late-type galaxies. Generally, early-type galaxies have smaller sizes than late-type galaxies, which was also reported by Shen et al. (2003); Courteau et al. (2007); Bottrell et al. (2017). To quantify the relation between galaxy size R_{50} and absolute magnitude M_r, we employ the following simple formula

$$R_{50} = \gamma L^{\alpha}(1 + L)^{(\beta - \alpha)} , \qquad (4)$$

where $L = 10^{-0.4(M_r - M_{r0})}$ is proportional to the luminosity, while α, β, γ and M_{r0} are four free fitting parameters. The method of least-squares is used to estimate the fitting parameters for the relation between the average galaxy size R_{50} and the r-band absolute magnitude M_r. The fitting results are shown as solid lines in Figure 1. For 214 950 early-type galaxies, we find that $\alpha = 0.26$, $\beta = 0.76$, $\gamma = 2.28$ and $M_{r0} = -21.8$ can provide a good fit to the data, while for 424 363 late-type galaxies, the fitting parameters are $\alpha = 0.31$, $\beta = 1.16$, $\gamma = 7.83$ and $M_{r0} = -23.5$. According to a comparison between the data and fitting results, we see that the model gives a very good description of the luminosity-size relations. In addition, one can see that the slopes of the luminosity-size relations show a prominent dependence on galaxy morphology. Generally, early-type galaxies have a deeper slope than late-type galaxies. This result is in qualitative agreement with a number of previous studies (e.g., Shen et al. 2003; Courteau et al. 2007; Dutton et al. 2011).

In addition to the absolute magnitudes, we also study the size distribution of galaxies as a function of stellar mass. The mass-size relations are shown in the right panel of Figure 1 as solid dots. To quantify the mass dependence of R_{50}, we fit the average mass-size relations by the following formula

$$R_{50} = \gamma \Big(\frac{M_*}{M_0}\Big)^{\alpha} \Big(1 + \frac{M_*}{M_0}\Big)^{(\beta - \alpha)} , \qquad (5)$$

where M_* is the stellar mass of the galaxy, α is the slope with stellar mass $M_* \ll M_0$, β is the slope with stellar mass $M_* \gg M_0$ and M_0 is the transition mass. Here, α, β, γ and M_0 are all fitting parameters. The least-squares method is used to fit these parameters. The fitting results are shown as solid curves in Figure 1.

For late-type galaxies (blue curve), the fitting parameters are $\alpha = 0.22$, $\beta = 1.24$, $\gamma = 8.83$ and $M_0 = 4.49 \times 10^{11} h^{-2} M_{\odot}$. For early-type galaxies (red curve),

the fitting parameters are $\alpha = 0.11$, $\beta = 0.60$, $\gamma = 1.75$ and $M_0 = 1.35 \times 10^{10} h^{-2} M_{\odot}$. The high-mass slope $\beta = 0.60$ of early-type galaxies is almost consistent with the slope 0.57 measured for quiescent high-mass galaxies $M_* > 10^{10.7} M_{\odot}$ from SDSS DR7 (Newman et al. 2012), and with the slope 0.58 measured from SDSS early-type galaxies with mass $M_* > 10^{10.5} M_{\odot}$ (Cimatti et al. 2012).

3.2 Dependence on Morphology

Next, we study the luminosity-size relation based on morphological classifications from GZ2 (Willett et al. 2013). The left panel of Figure 3 displays the luminosity-size relations for 107 230 elliptical (red) galaxies and 134 024 spiral (blue) galaxies. As shown in Figure 3, elliptical galaxies have a smaller size than spiral galaxies, which is similar to galaxy classifications according to the concentration c criterion in Figure 1. Equation (4) is also used to fit the $R_{50} - M_r$ relations, resulting in $\alpha = 0.19$, $\beta = 0.86$, $\gamma = 2.07$ and $M_{r0} = -21.5$ for elliptical galaxies and $\alpha = 0.26$, $\beta = 2.33$, $\gamma = 8.53$ and $M_{r0} = -24.5$ for spiral galaxies.

The right panel of Figure 3 depicts the size distribution of galaxies as a function of stellar mass. Here again, we use the least-squares method to fit these parameters in Equation (5). The fitting results are shown as the solid curves in Figure 3. For spiral galaxies, the fitting parameters are $\alpha = 0.16$, $\beta = 5.41$, $\gamma = 8.96$ and $M_0 = 1.93 \times 10^{12} h^{-2} M_{\odot}$. For elliptical galaxies, the fitting parameters are $\alpha = 0.13$, $\beta = 0.68$, $\gamma = 2.23$ and $M_0 = 2.96 \times 10^{10} h^{-2} M_{\odot}$. Overall, the mass-size relations for both spiral and elliptical galaxies follow the double power law distribution quite well. For elliptical galaxies, the low-mass galaxies ($M_* \ll M_0$) have $R_{50} \propto M_*^{0.13}$ and the high-mass galaxies ($M_* \gg M_0$) have $R_{50} \propto M_*^{0.68}$. van der Wel et al. (2014) also found a steep slope of 0.75 ± 0.06 for massive ($M_* > 2 \times 10^{10} M_{\odot}$) early-type galaxies at $z \sim 0.25$.

3.3 Dependence on Specific SFR

In addition to the concentration and morphology dependences, we also probe the luminosity-size relations for star-forming and quiescent galaxies. Using the best-fitting formula obtained by Chang et al. (2015, Equation (4)),

$$\log \Big[\text{sSFR}/(\text{yr}^{-1})\Big] = -0.2 \log \Big[M_*/(h^{-2} M_{\odot})\Big] - 8.94 ,$$
$$(6)$$

we separate galaxies in our sample into star-forming and quiescent subsamples. Apart from this separation criterion, we also test the separation criterion proposed by

Brinchmann et al. (2004), where galaxies are separated into two distinct populations using a constant sSFR value (e.g. $\log \text{sSFR} = -11.0$). We have checked our final results using a constant sSFR value to distinguish star-forming and quiescent galaxies, and found that the results are very similar to those using Equation (6).

Figure 4 shows the luminosity-size relations and mass-size relations for star-forming and quiescent galaxies in NYU-VAGC samples. The fitting parameters using Equation (4) and Equation (5) are listed in Table 1[2]. Generally, the sizes of star-forming galaxies are larger than those of quiescent galaxies. This result is expected due to the fact that star-forming galaxies are less concentrated, and quiescent galaxies are more concentrated (Brinchmann et al. 2004). Note that dwarf quiescent galaxies in the mass range $10^{8.0} \, h^{-2} \, M_\odot \le M_* < 10^9 \, h^{-2} \, M_\odot$ have larger sizes than galaxies with red solid points in the right panels of Figures 1, 3 and 5. This might be because dwarf quiescent galaxies, which have an exponential profile, are more likely to be separated into late-type galaxies using concentration as an indicator, while they are quiescent galaxies using sSFR as an indicator. As can be seen, both star-forming and quiescent galaxies can be fitted well by the double power law formula. Nevertheless, a single power law formula is also sufficient to describe the luminosity- or mass-size relations of star-forming galaxies. For example, the mass-size relation of star-forming galaxies can also be fitted well by $\log R_{50} = a \log M_* + b$, where $a = 0.24$ and $b = -1.75$.

3.4 Dependence on Bulge Fraction

In Simard et al. (2011)'s database, the galaxy image is fitted by the sum of a pure exponential disk and a de Vaucouleurs bulge. Using 586 938 galaxies cross identified from Simard et al. (2011)'s database, we further examine the dependence of the luminosity-size relation on the bulge fraction. In their canonical fitting model (bulge Sérsic index $n_b = 4$), Simard et al. (2011) used version 3.2 of the software package GIM2D to calculate the galaxy structural parameters, which are listed in table 1 of Simard et al. (2011). In this subsection, the structural parameters we used are the r-band galaxy circular half-light radius R_{chl} and the bulge fraction B/T. In Simard et al. (2011)'s database, the galaxy circular half-light radius R_{chl} is calculated by integrating GIM2D best-fit models with the summed bulge and disk profiles. Note that the bulge fraction can be best linked to the galaxy morphology to-

---

[2] For clarity, in what follows we only list the best fitting parameters in Table 1.

Table 1 Fitting Parameters

Case	α	β	γ	M_{r0}
Luminosity-size relation				
Early type	0.26	0.76	2.28	–21.8
Late type	0.31	1.16	7.83	–23.5
Elliptical	0.19	0.86	2.07	–21.5
Spiral	0.26	2.33	8.53	–24.5
Quiescent	0.17	0.80	2.57	–21.5
Star-forming	0.37	0.42	11.95	–23.9
$B/T \ge 0.5$	0.28	0.84	1.86	–21.4
$B/T < 0.5$	0.32	0.96	8.21	–23.6

Case	α	β	γ	M_0
Mass-size relation				
Early type	0.11	0.60	1.75	$1.35 \times 10^{10} \, h^{-2} \, M_\odot$
Late type	0.22	1.24	8.83	$4.49 \times 10^{11} \, h^{-2} \, M_\odot$
Elliptical	0.13	0.68	2.23	$2.96 \times 10^{10} \, h^{-2} \, M_\odot$
Spiral	0.16	5.41	8.96	$1.93 \times 10^{12} \, h^{-2} \, M_\odot$
Quiescent	–0.02	0.65	1.58	$1.11 \times 10^{10} \, h^{-2} \, M_\odot$
Star-forming	0.23	0.41	10.72	$4.90 \times 10^{11} \, h^{-2} \, M_\odot$
$B/T \ge 0.5$	0.14	0.71	1.53	$1.72 \times 10^{10} \, h^{-2} \, M_\odot$
$B/T < 0.5$	0.18	0.78	6.34	$1.57 \times 10^{11} \, h^{-2} \, M_\odot$

gether by the image smoothness (Simard et al. 2002, 2009). We have found that the luminosity-size relation is strongly dependent on the morphology, therefore a similar dependence on the bulge fraction is expected.

The left panel of Figure 5 shows the galaxy circular half-light radius as a function of r-band absolute magnitude of 586 938 galaxies cross identified in Simard et al. (2011)'s database. The relations of the galaxies with low ($B/T < 0.5$) and high ($B/T \ge 0.5$) bulge-to-total ratios are indicated by blue and red data points, respectively. The solid lines are the fitting results by Equation (4). The fitting parameters given by the least-squares method are listed in Table 1. As one can see, the size differences between low and high bulge fraction galaxies are somewhat similar to those of galaxies separated using different concentrations in Figure 1. At fixed absolute magnitude, the galaxies with higher bulge fraction B/T have smaller sizes. Besides, the luminosity-size relation with high bulge fraction ($B/T \ge 0.5$) has a steeper slope, especially for brighter galaxies ($M_r \le -20.5$). The right panel of Figure 5 displays the galaxy circular half-light radius as a function of stellar mass. The fitting results are shown as solid lines. The fitting parameters are also listed in Table 1. Similar to the luminosity-size relation, galaxies with high bulge fraction have steeper slope, especially for massive galaxies. This trend of increasing slope and decreasing sizes of the galaxies with higher bulge fraction agrees well with the results
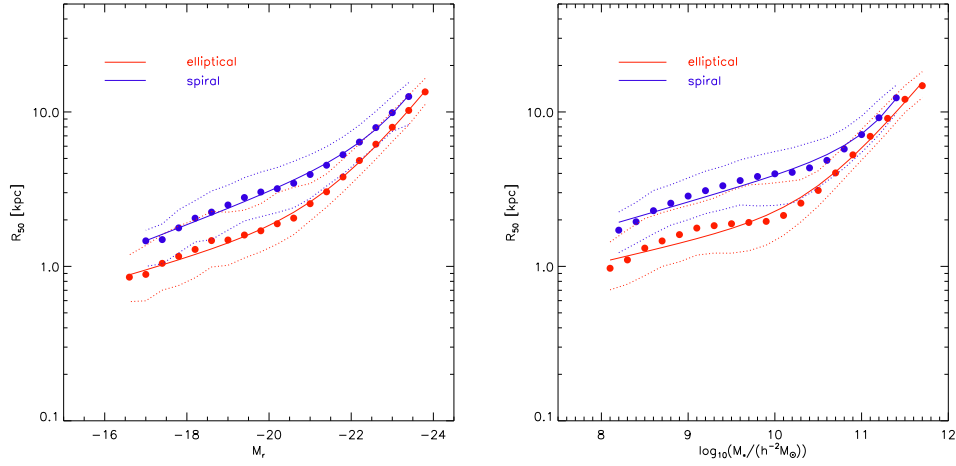
Fig. 3 Similar to Fig. 1, but for galaxy morphological classifications according to the GZ2 Catalog (Willett et al. 2013). The *red* and *blue data points* are median values of R_{50} for elliptical and spiral galaxies, respectively.
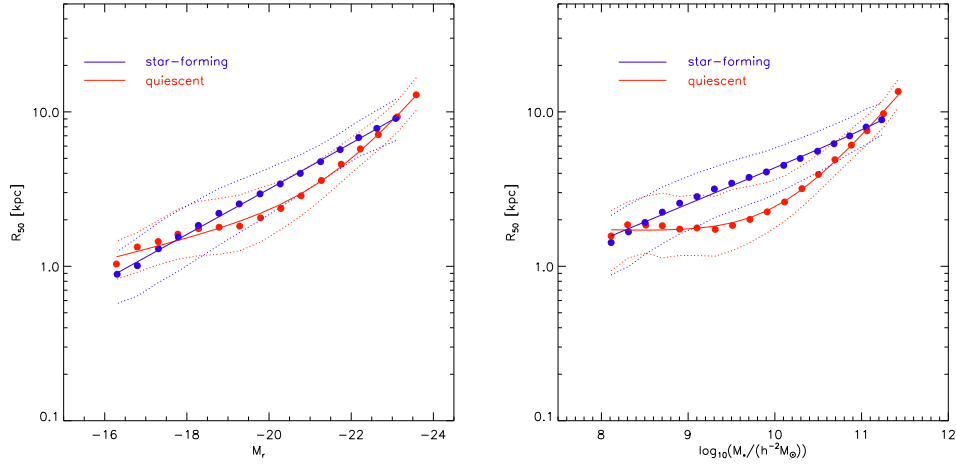

Fig. 4 Similar to Fig. 1, but for star-forming and quiescent galaxies. The *blue* and *red data points* are median values of R_{50} for star-forming and quiescent galaxies, respectively.
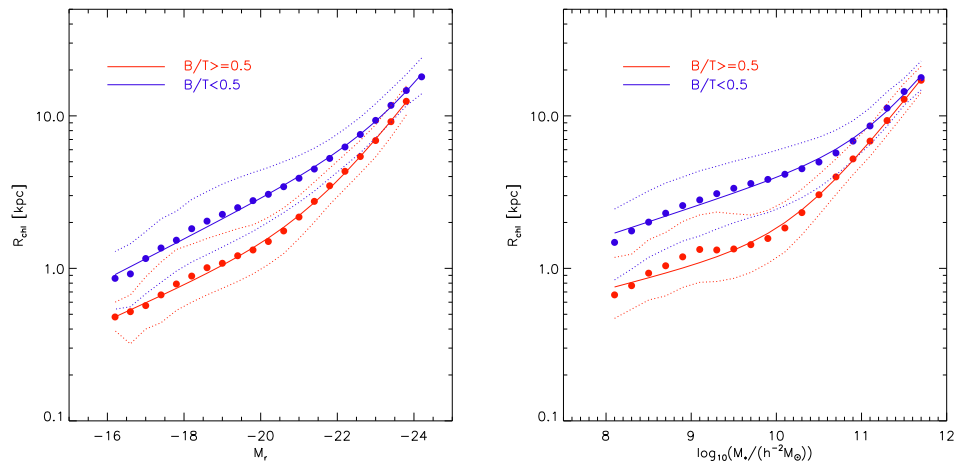

Fig. 5 Galaxy circular half-light radius R_{ch1} as a function of r-band absolute magnitude and stellar mass of galaxies cross identified with Simard et al. (2011)'s database. The *blue* and *red data points* are median values for galaxies with different r-band bulge fraction ($B/T < 0.5$ and $B/T \geq 0.5$). The *solid lines* show the fitting results using Eqs. (4) and (5), respectively.

of Bottrell et al. (2017) based on galaxy images from the Illustris simulation (Vogelsberger et al. 2014) and SDSS.

4 DEPENDENCE ON LARGE-SCALE ENVIRONMENT

Having modeled the luminosity- and mass-size relations for galaxies with different intrinsic properties, we proceed to probe their dependences on large scale environments. For simplicity, we only provide results based on the stellar mass of galaxies. Those of luminosities are very similar.

4.1 Dependence on Halo Environment

Note that all the results in this section are also investigated using early- or late-type galaxies. The results are very similar to those using all the galaxies. Therefore, in this section, we only present the results using all the galaxies for simplicity.

The first large scale environment we check is the halo environment. Based on the group catalog provided by Yang et al. (2007) from SDSS DR7, we separate the galaxies into centrals and satellites. Figure 6 shows the mass-size relations for central and satellite galaxies. Here we find that the central galaxies have slightly larger sizes in the mass range $10^{9.0} \, h^{-2} \, M_\odot \leq M_* < 10^{10.5} \, h^{-2} \, M_\odot$. This dependence disappears in galaxies beyond this mass range. In addition, as we have also tested by further separating the central and satellite galaxies into early-type or late-type sub-subsamples, the central/satellite dependence is quite similar. Using a sample of 911 central galaxies from SDSS DR4, Guo et al. (2009) also found that there are no size differences between early-type central and satellite galaxies, especially in the mass range $10^{10.5} \, h^{-2} \, M_\odot \leq M_* < 10^{11.25} \, h^{-2} \, M_\odot$ (see the upper-right panel of their figure 10). Huertas-Company et al. (2013) also claimed that central and satellite galaxies follow similar mass-size relations, based on $\sim 12\,000$ early-type galaxies with mass $10^{10.5} \, h^{-2} \, M_\odot \leq M_*$ in SDSS DR7.

In addition to the central/satellite separation, we also probe the mass-size relations for galaxies in high and low mass groups/halos. Based on the halo masses estimated by Yang et al. (2007) for galaxy groups in SDSS DR7, we separate the galaxies into two subsamples according to their halo mass. Figure 7 shows the mass-size relations of galaxies in halos with mass larger or smaller than $10^{13.0} \, h^{-1} \, M_\odot$. Here, we find galaxies in larger halos have smaller sizes in the stellar mass range $10^{9.0} \, h^{-2} \, M_\odot \leq M_* < 10^{10.5} \, h^{-2} \, M_\odot$. This is expected because those galaxies with $10^{9.0} \, h^{-2} \, M_\odot \leq M_* < 10^{10.5} \, h^{-2} \, M_\odot$ in halos larger than $10^{13.0} \, h^{-1} \, M_\odot$ are more likely to belong to satellite galaxies. Therefore, the results in Figures 6 and 7 are consistent.

4.2 Dependence on Cosmic Web Environment

The second large scale environment we check is the cosmic web. As mentioned before, galaxies in the NYU-VAGC samples can be classified into one of four cosmic web types: `cluster`, `filament`, `sheet` and `void`, according to the number of positive eigenvalues associated with the local tidal tensor $T_{i,j}$ constructed by Wang et al. (2012).

In this section, galaxies are further separated into early- and late-type galaxies according to their concentrations. Besides, galaxies are also divided into 'red' and 'blue' according to their $^{0.1}(g - r)$ colors: galaxies with $^{0.1}(g - r) \geq 0.83$ are called red galaxies, while galaxies with $^{0.1}(g - r) < 0.83$ are called blue galaxies. The value 0.83 roughly corresponds to the bimodal scale in the color-magnitude relation.

Figure 8 shows the mass-size relations of early- and late-type galaxies, which are separated into different cosmic web types. The solid points in different colors are the median sizes of galaxies in different environments: `cluster` (red), `filament` (orange), `sheet` (green) and `void` (blue). As one can see, there is no significant dependence of mass-size relations on the large-scale environment either for early- or late-type galaxies. For early-type galaxies in the mass range of $10^9 \, h^{-2} \, M_\odot \leq M_* < 10^{10} \, h^{-2} \, M_\odot$, the slight difference of galaxies in terms of different cosmic web types may be caused by the statistical uncertainty due to the sparsity of galaxies in each mass bin. For late-type galaxies in the mass range of $10^9 \, h^{-2} \, M_\odot \leq M_* < 10^{10} \, h^{-2} \, M_\odot$, we can barely see that the galaxies in `cluster` are slightly smaller than those in the other three cosmic web environments.

Figure 9 shows the mass-size relations of red and blue galaxies in different cosmic web environments. As one can see, there is almost no difference for red or blue samples in terms of different cosmic web types.

4.3 Dependence on Local Number Density

The last large scale environment we check is the local galaxy number density. We investigate the dependence of the mass-size relation on the local galaxy surface number density as defined in Equation (3). We have used several sets of parameters of $r = (1, 2, 5, 10) \, h^{-1} \, \mathrm{Mpc}$ and $\Delta v = \pm(500, 1000) \, \mathrm{km \, s^{-1}}$ to calculate the galaxy surface num-
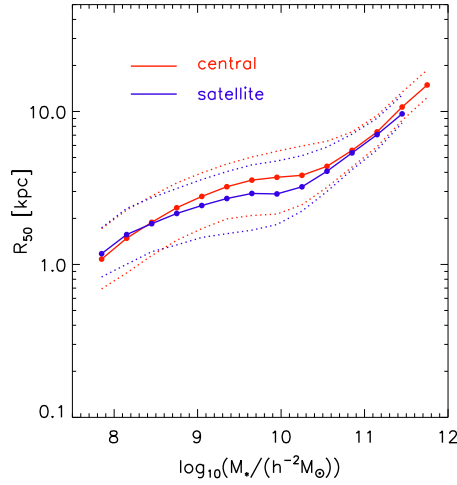
Fig. 6 Galaxy Petrosian half-light radius R_{50} as a function of stellar mass for central and satellite galaxies.
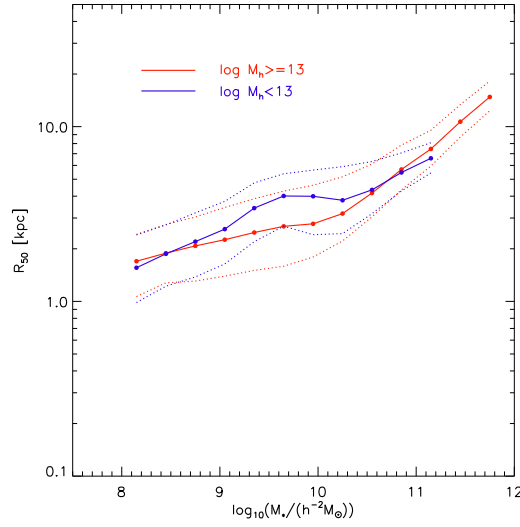

Fig. 7 Galaxy Petrosian half-light radius R_{50} as a function of stellar mass for galaxies in halos with mass larger or smaller than $10^{13.0} \, h^{-1} \, M_{\odot}$.
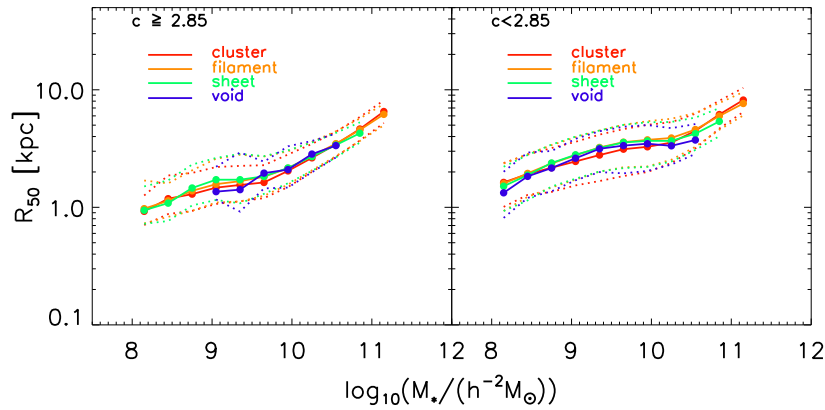

Fig. 8 Mass-size relations of early- ($c \geq 2.85$) and late-type ($c < 2.85$) galaxies in different environments, indicated by different colors: `cluster` (*red*), `filament` (*orange*), `sheet` (*green*) and `void` (*blue*).
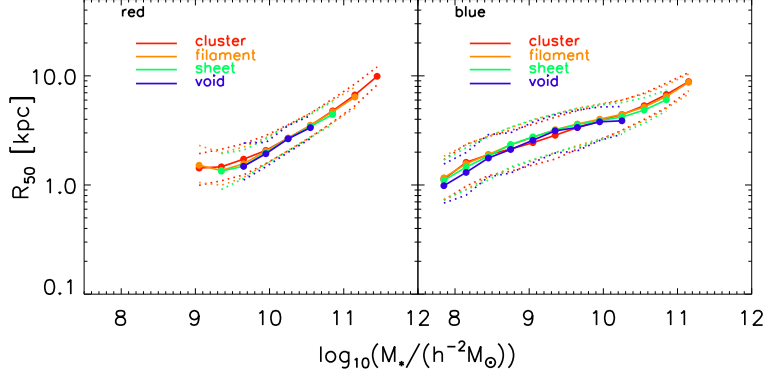
Fig. 9 Same as Fig. 8, but for red and blue galaxies.
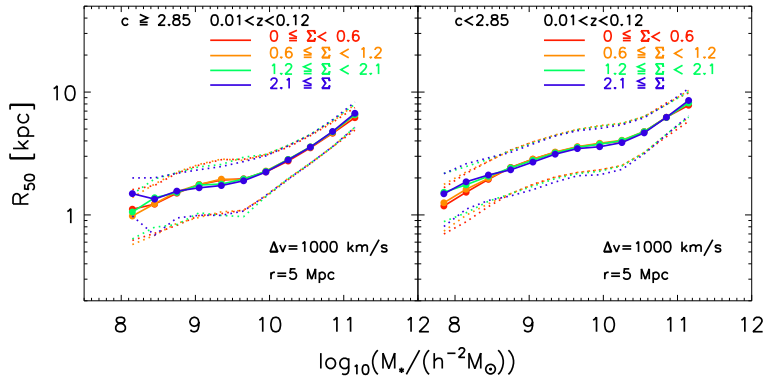
Fig. 10 Mass-size relations for early- and late-type galaxies in different galaxy surface number density environments, measured by galaxy counts in cylinders with $r = 5\,h^{-1}\,\mathrm{Mpc}$ and $\Delta v = \pm 1000\,\mathrm{km\,s^{-1}}$.
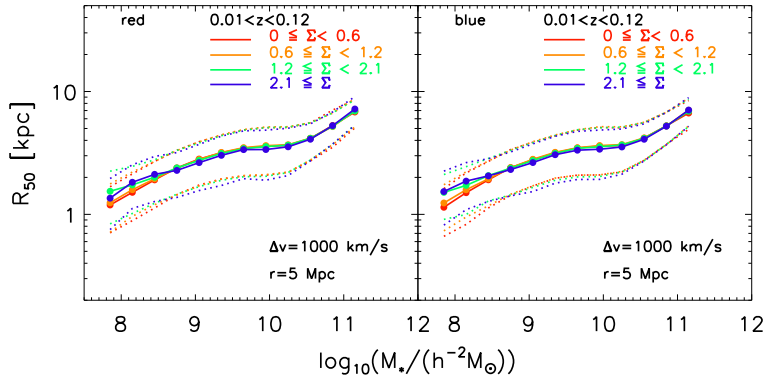
Fig. 11 Same as Fig. 10, but for red and blue galaxies.

ber density. Our main conclusion is not changed using different r or Δv. Based on the surface number densities calculated using $r = 5\,h^{-1}\,\mathrm{Mpc}$ and $\Delta v = 1000\,\mathrm{km\,s^{-1}}$, we divide galaxies into four equal subsamples according to their surface number densities: (1) $0 < \Sigma < 0.6$, (2) $0.6 \leq \Sigma < 1.2$, (3) $1.2 \leq \Sigma < 2.1$ and (4) $\Sigma \geq 2.1$. Besides, we

have separated galaxies into early- and late-type samples (red and blue samples) as was done in Section 4.2.

Figure 10 shows the mass-size relations of early- and late-type galaxies in different surface number density environments. We find that the sizes in different surface number density environments are almost the same either for

early-type galaxies or for late-type galaxies. The slight difference for galaxies with mass $M_* < 10^{8.5} \, h^{-2} \, M_\odot$ should be due to the statistical uncertainty induced by the sparse number in these mass bins. Figure 11 shows the mass-size relations for red and blue galaxies. As can be seen, the sizes of galaxies with different surface number densities are also the same in the mass range $M_* \geq 10^{8.5} \, h^{-2} \, M_\odot$.

5 SUMMARY

Using a sample of 639 359 galaxies selected from SDSS DR7 and a catalog of bulge-disk decompositions, we examine the size distribution of galaxies and its dependence on the intrinsic properties of galaxies, such as concentration, morphology, sSFR and bulge fraction, and on the large-scale environments in the context of central/satellite decomposition, halo environment, the cosmic web: `cluster`, `filament`, `sheet` and `void`, as well as galaxy surface number density.

In order to investigate the dependence of the morphology, the galaxies are separated into early- and late-type galaxies using the concentration index $c = 2.85$. Besides, we also separate galaxies into elliptical and spiral cases using the morphological classifications from GZ2. In addition to these, as the sSFR and bulge fraction of the galaxy can be linked to galaxy morphology, we also separate the galaxies into low/high sSFR and high/low bulge fraction samples.

A double power law fitting formula has been used to quantify the relations between the logarithm of the galaxy size and the r-band absolute magnitude as well as the stellar mass. The related best fitting parameters are provided in Table 1. There is a clear trend that galaxy size increases with galaxy luminosity and stellar mass. Early-type (elliptical) galaxies have smaller sizes than late-type (spiral) galaxies. There is a strong dependence of luminosity (stellar mass)-size relation on the galaxy morphology, with steeper slopes for early-type (elliptical) galaxies. As expected, the size differences between low ($B/T < 0.5$) and high (B/T) bulge fraction are somewhat similar to those of galaxies separated according to their morphological classifications. There is a trend of increasing slope and decreasing sizes for galaxies with high bulge fraction.

A number of efforts have been made to investigate the large scale environmental dependence of the size distribution of galaxies. On one hand, some studies claimed that there is no environmental dependence in the mass-size relation (Maltby et al. 2010; Nair et al. 2010; Huertas-Company et al. 2013; Kelkar et al. 2015; Saracco et al.

2017). On the other hand, there are some studies suggesting that the sizes of galaxies are dependent on their environments (Papovich et al. 2012; Bassett et al. 2013; Lani et al. 2013; Strazzullo et al. 2013; Delaye et al. 2014; Yoon et al. 2017).

In this paper, we examine the environmental dependence of the mass-size (luminosity-size) relations of galaxies in SDSS DR7 with much larger volumes and numbers of galaxies. Galaxies are separated into centrals and satellites, and separated into high mass and low mass halo environments. We do find that galaxies in the stellar mass range $10^{9.0} \, h^{-2} \, M_\odot \leq M_* < 10^{10.5} \, h^{-2} \, M_\odot$ have a weak but prominent halo environment dependence. The satellites and those in massive halos have somewhat smaller sizes than their counterparts. Beyond this stellar mass range, we do not see any halo environmental dependence.

For the cosmic web, we find that there is almost no significant difference in size for galaxies that are separated into four cosmic web environments: `cluster`, `filament`, `sheet` and `void`. Furthermore, we investigate the dependence of the mass-size relation on the local galaxy surface number density. Galaxies are then separated into four equal subsamples according to their surface number densities. We find that galaxies with different surface number densities have almost the same sizes.

Astrophysics, Instituto de Astrofísica de Canarias, The Johns Hopkins University, Kavli Institute for the Physics and Mathematics of the Universe (IPMU)/University of Tokyo, Lawrence Berkeley National Laboratory, Leibniz Institut für Astrophysik Potsdam (AIP), Max-Planck-Institut für Astronomie (MPIA Heidelberg), Max-Planck-Institut für Astrophysik (MPA Garching), Max-Planck-Institut für Extraterrestrische Physik (MPE), National Astronomical Observatories of China, New Mexico State University, New York University, University of Notre Dame, Observatório Nacional/MCTI, The Ohio State University, Pennsylvania State University, Shanghai Astronomical Observatory, United Kingdom Participation Group, Universidad Nacional Autónoma de México, University of Arizona, University of Colorado Boulder, University of Oxford, University of Portsmouth, University of Utah, University of Virginia, University of Washington, University of Wisconsin, Vanderbilt University and Yale University.

References

Abazajian, K. N., Adelman-McCarthy, J. K., Agüeros, M. A., et al. 2009, ApJS, 182, 543

Bassett, R., Papovich, C., Lotz, J. M., et al. 2013, ApJ, 770, 58

Bernardi, M., Roche, N., Shankar, F., & Sheth, R. K. 2011, MNRAS, 412, L6

Blanton, M. R., Dalcanton, J., Eisenstein, D., et al. 2001, AJ, 121, 2358

Blanton, M. R., Brinkmann, J., Csabai, I., et al. 2003, AJ, 125, 2348

Blanton, M. R., Schlegel, D. J., Strauss, M. A., et al. 2005, AJ, 129, 2562

Blanton, M. R., & Roweis, S. 2007, AJ, 133, 734

Bottrell, C., Torrey, P., Simard, L., & Ellison, S. L. 2017, MNRAS, 467, 2879

Brinchmann, J., Charlot, S., White, S. D. M., et al. 2004, MNRAS, 351, 1151

Buitrago, F., Trujillo, I., Conselice, C. J., et al. 2008, ApJ, 687, L61

Cappellari, M., McDermid, R. M., Alatalo, K., et al. 2013, MNRAS, 432, 1862

Cebrián, M., & Trujillo, I. 2014, MNRAS, 444, 682

Chan, J. C. C., Beifiori, A., Mendel, J. T., et al. 2016, MNRAS, 458, 3181

Chang, Y.-Y., van der Wel, A., da Cunha, E., & Rix, H.-W. 2015, ApJS, 219, 8

Cimatti, A., Nipoti, C., & Cassata, P. 2012, MNRAS, 422, L62

Courteau, S., Dutton, A. A., van den Bosch, F. C., et al. 2007, ApJ, 671, 203

de Jong, R. S., & Lacey, C. 2000, ApJ, 545, 781

Delaye, L., Huertas-Company, M., Mei, S., et al. 2014, MNRAS, 441, 203

Deng, X.-F. 2013, RAA (Research in Astronomy and Astrophysics), 13, 651

Deng, X.-F., & Yu, G. 2015, Astrophysics, 58, 250

Desroches, L.-B., Quataert, E., Ma, C.-P., & West, A. A. 2007, MNRAS, 377, 402

Dutton, A. A., van den Bosch, F. C., Dekel, A., & Courteau, S. 2007, ApJ, 654, 27

Dutton, A. A., van den Bosch, F. C., Faber, S. M., et al. 2011, MNRAS, 410, 1660

Fall, S. M. 1983, in IAU Symposium, 100, Internal Kinematics and Dynamics of Galaxies, ed. E. Athanassoula, 391

Fall, S. M., & Efstathiou, G. 1980, MNRAS, 193, 189

Fall, S. M., & Romanowsky, A. J. 2013, ApJ, 769, L26

Forero-Romero, J. E., Hoffman, Y., Gottlöber, S., Klypin, A., & Yepes, G. 2009, MNRAS, 396, 1815

Furlong, M., Bower, R. G., Crain, R. A., et al. 2017, MNRAS, 465, 722

Guo, Y., McIntosh, D. H., Mo, H. J., et al. 2009, MNRAS, 398, 1129

Hahn, O., Carollo, C. M., Porciani, C., & Dekel, A. 2007a, MNRAS, 381, 41

Hahn, O., Porciani, C., Carollo, C. M., & Dekel, A. 2007b, MNRAS, 375, 489

Hill, A. R., Muzzin, A., Franx, M., et al. 2017, ApJ, 837, 147

Hopkins, P. F., Bundy, K., Hernquist, L., Wuyts, S., & Cox, T. J. 2010, MNRAS, 401, 1099

Huertas-Company, M., Mei, S., Shankar, F., et al. 2013, MNRAS, 428, 1715

Hyde, J. B., & Bernardi, M. 2009, MNRAS, 394, 1978

Javanmardi, B., & Kroupa, P. 2017, A&A, 597, A120

Kelkar, K., Aragón-Salamanca, A., Gray, M. E., et al. 2015, MNRAS, 450, 1246

Khochfar, S., & Silk, J. 2006, ApJ, 648, L21

Lange, R., Driver, S. P., Robotham, A. S. G., et al. 2015, MNRAS, 447, 2603

Lange, R., Moffett, A. J., Driver, S. P., et al. 2016, MNRAS, 462, 1470

Lani, C., Almaini, O., Hartley, W. G., et al. 2013, MNRAS, 435, 207

Maltby, D. T., Aragón-Salamanca, A., Gray, M. E., et al. 2010, MNRAS, 402, 282

Mo, H. J., Mao, S., & White, S. D. M. 1998, MNRAS, 295, 319

Nair, P. B., van den Bergh, S., & Abraham, R. G. 2010, ApJ, 715, 606

Nakamura, O., Fukugita, M., Yasuda, N., et al. 2003, AJ, 125, 1682

Newman, A. B., Ellis, R. S., Bundy, K., & Treu, T. 2012, ApJ, 746, 162

Papovich, C., Bassett, R., Lotz, J. M., et al. 2012, ApJ, 750, 93

Park, C., & Choi, Y.-Y. 2005, ApJ, 635, L29

Peebles, P. J. E. 1969, ApJ, 155, 393

Planck Collaboration, Ade, P. A. R., Aghanim, N., et al. 2016, A&A, 594, A13

Poggianti, B. M., Calvi, R., Bindoni, D., et al. 2013, ApJ, 762, 77

Pranger, F., Trujillo, I., Kelvin, L. S., & Cebrián, M. 2017,

MNRAS, 467, 2127

Raichoor, A., Mei, S., Stanford, S. A., et al. 2012, ApJ, 745, 130

Rettura, A., Rosati, P., Nonino, M., et al. 2010, ApJ, 709, 512

Romanowsky, A. J., & Fall, S. M. 2012, ApJS, 203, 17

Saracco, P., Gargiulo, A., Ciocca, F., & Marchesini, D. 2017, A&A, 597, A122

Shen, S., Mo, H. J., White, S. D. M., et al. 2003, MNRAS, 343, 978

Shimasaku, K., Fukugita, M., Doi, M., et al. 2001, AJ, 122, 1238

Simard, L., Willmer, C. N. A., Vogt, N. P., et al. 2002, ApJS, 142, 1

Simard, L., Clowe, D., Desai, V., et al. 2009, A&A, 508, 1141

Simard, L., Mendel, J. T., Patton, D. R., Ellison, S. L., & McConnachie, A. W. 2011, ApJS, 196, 11

Strazzullo, V., Gobat, R., Daddi, E., et al. 2013, ApJ, 772, 118

Sweet, S. M., Sharp, R., Glazebrook, K., et al. 2017, MNRAS, 464, 2910

Trujillo, I., Rudnick, G., Rix, H.-W., et al. 2004, ApJ, 604, 521

Trujillo, I., Förster Schreiber, N. M., Rudnick, G., et al. 2006, ApJ, 650, 18

Trujillo, I., Conselice, C. J., Bundy, K., et al. 2007, MNRAS, 382, 109

van der Wel, A., Holden, B. P., Zirm, A. W., et al. 2008, ApJ, 688, 48

van der Wel, A., Franx, M., van Dokkum, P. G., et al. 2014, ApJ, 788, 28

Vogelsberger, M., Genel, S., Springel, V., et al. 2014, MNRAS, 444, 1518

Wang, H., Mo, H. J., Yang, X., & van den Bosch, F. C. 2012, MNRAS, 420, 1809

White, S. D. M. 1984, ApJ, 286, 38

White, S. D. M., & Rees, M. J. 1978, MNRAS, 183, 341

Willett, K. W., Lintott, C. J., Bamford, S. P., et al. 2013, MNRAS, 435, 2835

Yang, X., Mo, H. J., van den Bosch, F. C., & Jing, Y. P. 2005, MNRAS, 356, 1293

Yang, X., Mo, H. J., van den Bosch, F. C., et al. 2007, ApJ, 671, 153

Yasuda, N., Fukugita, M., Narayanan, V. K., et al. 2001, AJ, 122, 1104

Yıldırım, A., van den Bosch, R. C. E., van de Ven, G., et al. 2017, MNRAS, 468, 4216

Yoon, Y., Im, M., & Kim, J.-W. 2017, ApJ, 834, 73

York, D. G., Adelman, J., Anderson, Jr., J. E., et al. 2000, AJ, 120, 1579

Zhang, Y., Yang, X., Faltenbacher, A., et al. 2009, ApJ, 706, 747

Zhang, Y., Yang, X., Wang, H., et al. 2013, ApJ, 779, 160

Zhang, Y., Yang, X., Wang, H., et al. 2015, ApJ, 798, 17